2024 NDIA MICHIGAN CHAPTER
GROUND VEHICLE SYSTEMS ENGINEERING
AND TECHNOLOGY SYMPOSIUM
POWER AND MOBILITY TECHNICAL SESSION
AUGUST 13-15, 2024 - NOVI, MICHIGAN

Permanent Magnet Synchronous Motor (PMSM) Performance Characterization in a Hybrid-Electric Propulsion System

Erik Schroen[1], Constandinos Mitsingas[1], Chol-Bum "Mike" Kweon[1]

[1]DEVCOM Army Research Laboratory, Aberdeen Proving Ground, MD, USA, 21005

ABSTRACT

The paper characterizes and documents the performance evaluation of an electric motor and motor controller/inverter. An overall energy balance on the electric motor itself was performed that resulted in a maximum operating efficiency of 94%, while the combined motor and motor controller/inverter system resulted in an 80% efficiency at 2,500 RPM and 60 Nm operating conditions. The zero load power requirements were identified across a span of operating conditions and compared against manufacturer provided values. Vibrations in the system were shown to impact motor control, through the current draw values, that resulted in unstable operation regimes.

Citation: E. Schroen, C. Mitsingas, C.B. Kweon, "Permanent Magnet Synchronous Motor (PMSM) Performance Characterization in a Hybrid-Electric Propulsion System," In *Proceedings of the Ground Vehicle Systems Engineering and Technology Symposium* (GVSETS), NDIA, Novi, MI, Aug. 13-15, 2024.

1. INTRODUCTION

In the advent of electrification, the use of electric machines, particularly electric motors and motor controllers/inverters, have been made more broadly available. In particular, electrification has greatly opened up the design space for both ground and aerial vehicles, allowing for some unique designs, ranging from multi-rotors to tail sitters to tilt-rotors [1, 2].

The electric motor and inverter pair play a critical role for the whole system, as they handle the electric and mechanical power conversions. Of particular importance is the specific power of the electric machines which dominates the mass of the electric-propulsion system. Current motor technologies have been able to achieve up to 10 kW/kg for aviation applications [3]. In addition, electric machines promise a reduction in overall CO2 emissions by increasing the overall efficiency of standalone engine system when converted to a hybrid configuration [4].

However, a lot of the rated properties for these electric machines are not well understood, nor how to effectively use them to achieve the performance necessary to enable hybridization.

In this paper, an EMRAX 228 electric motor in combination with a UniTek Bamocar D3 inverter is evaluated under a

broad range of conditions, with a goal to determine its individual and overall system efficiency, as well as observe how the system efficiency changes with a decrease in the DC bus voltage, which would reflect a draining battery system and inform initial vehicle bus voltage selection for optimized performance. This facility could be used as a platform to evaluate propulsion systems for both aviation and ground vehicles.

2. Experimental Apparatus

The experimental setup is shown in figure 1. Figure 1 shows a top view of the experimental setup (Left), including two dynamometers, EMRAX 228 electric motor, and a combining gearbox. A schematic of the full system layout, including the power, coolant, and mechanical connections is shown in Figure 1 (Right).

The load and driving dynamometers are AC induction motors from PTI Instruments, powered by ABB Variable Frequency Drives (VFD). The load dynamometer can produce or absorb 149 kW of mechanical power with a maximum speed of 6,000 RPM, while the driving dynamometer can produce 149 kW of mechanical power with a maximum of 12,000 RPM. The EMRAX motor can provide a continuous mechanical power of 62 kW at 5,500 RPM with a maximum of 109 kW for short durations and is controlled using a UniTek Bamocar D3 inverter. The inverter is powered from a Regatron DC power supply that is capable of both sourcing and sinking electrical power to emulate battery performance. A 1:2 speed-reducing combining gearbox combines the inputs of the driving dynamometer and EMRAX motor to a single output to the load dynamometer. An oil lubrication cart is used to both lubricate and cool the spur gears in the combining gearbox. Each input and output shaft has an HBM T40B torque transducer. Each dynamometer shaft utilizes a gearwheel encoder, and the EMRAX motor utilizes a resolver for speed determination.

Electrical breakout boxes are used between the Regatron power supply and inverter, and between the inverter and EMRAX. The breakout boxes include phase-to-phase voltage and phase current sensors (Verivolt) for each phase in each box. This allows for the measurement of the DC power consumed by the motor and controller, as well the AC power consumed by the motor itself. Cables between the breakout box and motor were kept short, ~1 m, to minimize cable losses.

The EMRAX is liquid cooled using a 50% ethylene glycol and 50% water mixture. Flow goes from the heat exchanger, between the local cooling loop and building cooling loop, to the EMRAX followed by the UniTek, and then into a reservoir. A flow meter is used to measure the coolant flow rate, and temperature sensors are installed in the liquid entrance and exit to both the EMRAX and

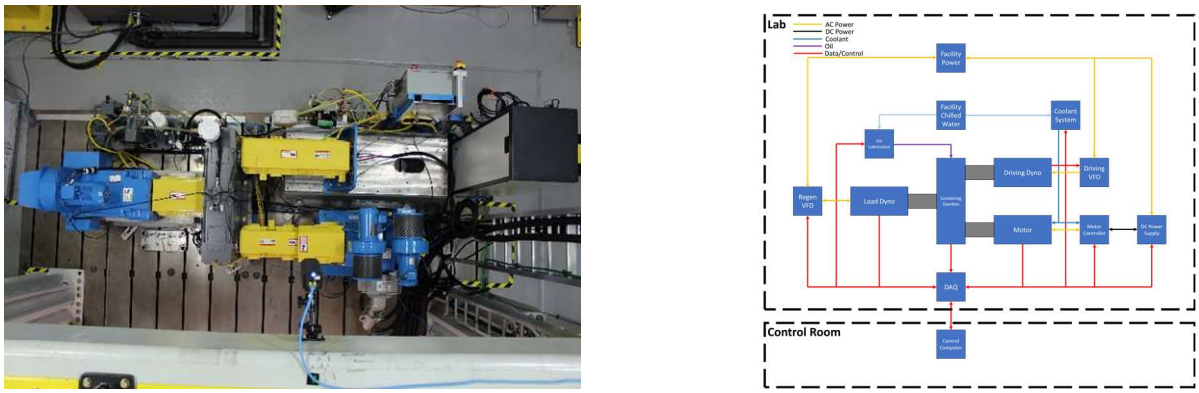

Figure 1: (Left) Experimental setup and (Right) component layout diagram.

Unitek. This allows for the calculation of waste heat produced by both components.

Single-axis accelerometers are located on the combining gearbox inputs and output and each rotating machine. An additional three-axis accelerometer was added to the EMRAX motor tombstone.

The system can be operated in different control modes. The first control mode is using the load dynamometer to set the torque setpoint and then using the driving dynamometer to set the speed of the system, allowing the EMRAX motor to operate in a torque-control mode. The driving dynamometer provides the difference in power between the load dynamometer and EMRAX motor to maintain the speed setpoint. The second control mode uses the EMRAX motor in speed-control mode to set the speed of the system and uses the load dynamometer to set the total torque of the system. The EMRAX motor provides the power necessary to maintain the speed setpoint. In this configuration the driving dynamometer is decoupled.

3. Experimental Methodology

A control volume of the EMRAX is shown in figure 2. The energy balance around the motor control volume shows that the electrical energy in, should equal the mechanical energy out plus the energy lost as heat.

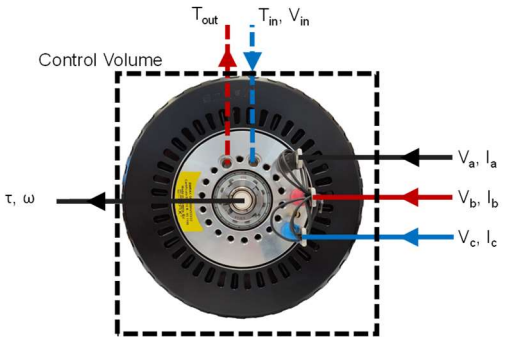

Figure 2: Control volume around EMRAX motor, for electrical power in, mechanical power out and heat loss.

The input electrical power to the motor can be calculated using Blondel's Theorem using the phase currents and the line-to-line voltages of the 3-phase system. Using a single phase (W) as the common voltage reference points allows for the power to be calculated from the current in the remaining two phases (U & V), shown in equations 1 & 2.

$$P_1 = i_U * e_{UW}\ [kW] \quad (1)$$

$$P_2 = i_V * e_{VW}\ [kW] \quad (2)$$

Where P is the instantaneous electrical power, i is the instantaneous phase current in amps, and e is the instantaneous line-to-line voltage in volts. The total three phase power is then the sum of the two powers, shown in equation 3.

$$P_T = P_1 + P_2\ [kW] \quad (3)$$

The heat loss from the motor is rejected into the cooling fluid and therefore, can be expressed as a function of the cooling fluid density in kg/m^3, ρ, flow rate in m^3/s, υ, specific heat in kJ/(kg*K, Cp, and temperature change across the motor in °C, T, as shown in equation 4.

$$Q_{loss} = \rho * \upsilon * Cp * (T_{out} - T_{in})\ [kW] \quad (4)$$

The mechanical power of the motor is determined by multiplying the measured torque in Nm, τ, and speed in RPM, ω, as described by equation 3.

$$P_{mech} = \frac{\tau * \omega}{9548.8}\ [kW] \quad (3)$$

4. Results and Discussion

In this section, the EMRAX motor and UniTek inverter are evaluated in terms of their power conversion capabilities. The motor is first tuned to operate in the experimental setup discussed prior and its zero load losses are determined. The current and vibration profiles of the motor are explored for different operating conditions,

before determining the efficiency contour of the motor and controller/inverter.

4.1. EMRAX PID Tunning

In Figure 3, the EMRAX response for a given speed setpoint change can be observed, using the manufacturer provided tuning file.

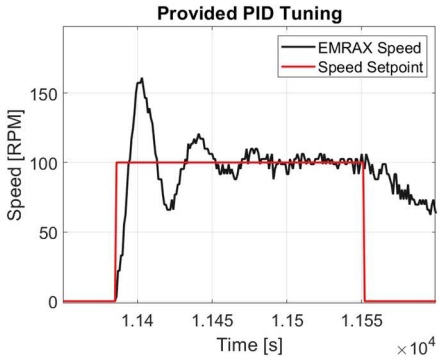

Figure 3: EMRAX response to a speed setpoint using provided tunning parameters.

The motor was then tuned for the system described here, with the final results shown in Figure 4. No derivative control was used, and the proportional and integral values were changed both for the speed and current controllers.

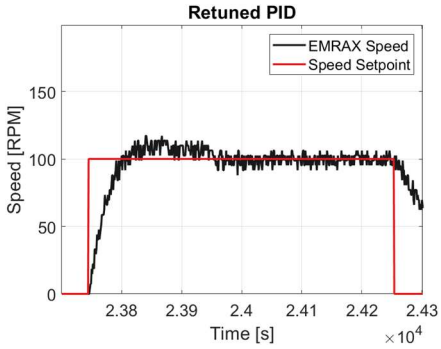

Figure 4: EMRAX response to a speed setpoint after tunning.

Figure 5 shows the EMRAX response for a larger band of speed sepoints. The motor is able to respond fast and accurately to the setpoints with minimal overshoot. The maximum motor ramp rate was set to 5,000 RPM/s.

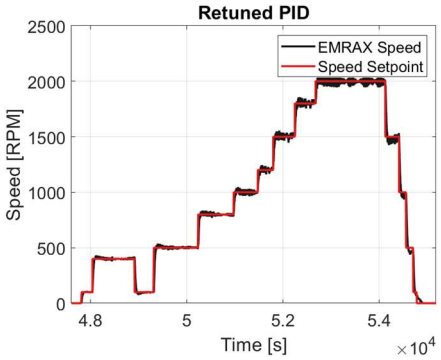

Figure 5: Retuned EMRAX response to a speed setpoint.

4.2. EMRAX Free Run Losses

The EMRAX was operated at different speeds while decoupled from the system and with no mechanical loading in order to determine the no-load losses of the motor.

In Figure 6, the zero load losses of the motor are shown, including both with the Unitek controller being on and off, as well as whether the rotational speed was increasing or decreasing during the experiment. This was accomplished by using the driving dynamometer to drive system, therefore not requiring the Unitek to be active.

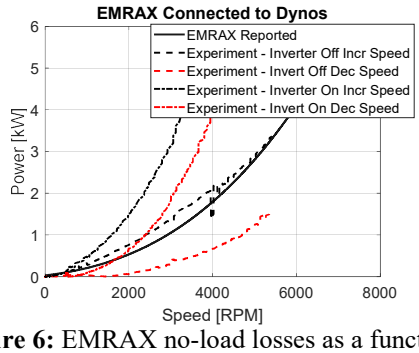

Figure 6: EMRAX no-load losses as a function of speed and whether Unitek controller/inverter is operational.

Two major observations were made, with the first one being that whether the Unitek controller was on or off, greatly impacted the zero load losses of the EMRAX. This was determined to be due to active rectification of the inverter in the attempt to maintain the zero torque setpoint, creating mechanical

drag on the motor. The second observation was a hysteresis that existed, depending on whether the EMRAX rotational speed was increasing or decreasing. In general, for both cases the zero load losses were lower when decreasing in speed, compared to when increasing in speed. The zero load losses reported by the manufacturer match best with the inverter disabled and increasing speed case.

The EMRAX motor was then completely disconnected from the dynamometers and left to freely rotate in space. In this case, the Unitek controller is operational and the results are shown in Figure 7. The no-load losses are shown to be different depending on whether the EMRAX speed is increasing or decreasing. However, in this case, the motor was left to reach steady state conditions for several speeds. During those cases, it was observed that the zero load losses would reach an intermediate value between the two curves, shown by the larger grouping of data points in the figure. The zero load losses reported by the manufacturer match best to the case that the EMRAX was free spinning and decreasing in speed.

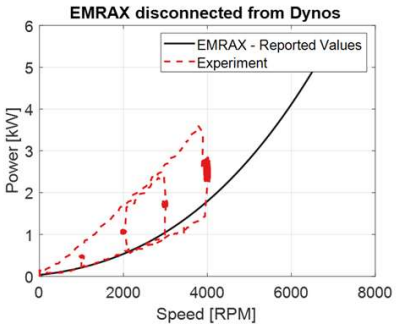

Figure 7: EMRAX no-load losses as a function of speed, disconnected from system.

4.3. EMRAX Current and Vibrations

For evaluating system vibrations, the motor was operating at both steady state and transient operation. The speed setpoints for both of these are shown in Figure 8 for a maximum operating speed of 5,550 RPM.

For the first segment, speed is slowly increased (~500 RPM/step) to 4,500 RPM,

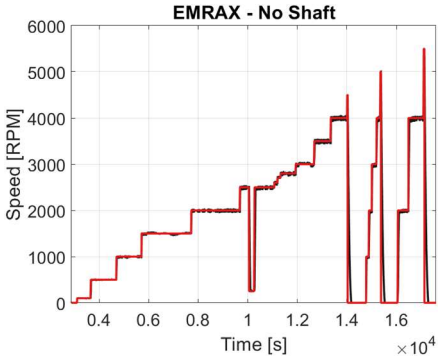

Figure 8: EMRAX setpoint and actual speed.

after which the motor controller detected an overcurrent condition and disabled. Following the second segment, the speed is increased by a larger step (~1,000 RPM/step) and a similar phenomenon is observed at 5,000 RPM. On the last segment the step increase is 2,000 RPM/step until the last step from 4,000 RPM to 5,500 RPM, where a similar overcurrent condition is observed.

Figure 9 shows the different phase currents of the motor as well as the DC current provided by the power supply for three

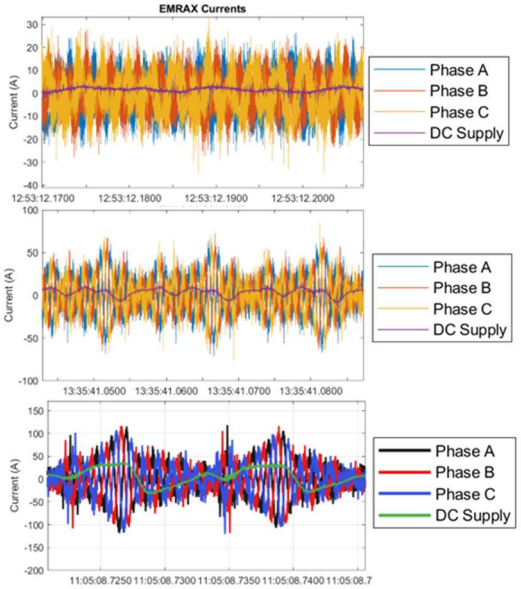

Figure 9: EMRAX phase current and DC power supply current profiles for Top 2,000 RPM, middle 4,000 RPM and bottom 4,800 RPM.

different speeds (2,000 RPM, 4,000 RPM and 4,800 RPM).

It can be observed that, as the motor speed increases, the current waveforms begin to depart from a sinusoidal curve, showing lower-order frequencies. This is more evident in the DC current profile, which is fairly steady at 2,000 RPM and transitions to an oscillatory profile by the time the motor reaches 4,800 RPM. This indicates that the inverter is having difficulty maintaining the appropriate motor setpoints in part due to the larger system vibrations at higher speeds. The observed motor vibrations as a function of speed are shown in Figure 10. Clear resonant frequencies are observed at around 600 RPM, 3,200 RPM and 4,600 RPM. The baseline vibrations also increased with increasing motor speed.

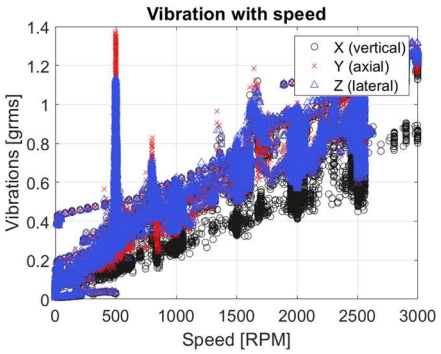

Figure 10: EMRAX 3-axis vibrations as a function of speed.

4.4. EMRAX Motor Efficiency

The motor efficiency calculated, as described in the experimental section, is shown in Figure 11, as a function of applied torque and speed. It can be observed that the highest efficiency of 94% is obtained when the motor is operating at medium speeds (~2,500 RPM) and medium-high torques (60 Nm).

Figure 12 shows the combined motor and inverter system efficiency at the maximum DC bus voltage of 680 V. It is observed that the system efficiency drastically drops to a maximum of 80%, and the efficiency contours appear to move closer to lower speeds and higher torques. This is because the inverter duty cycle is longer at higher torques and is able to finer control the current per motor revolution at lower speeds.

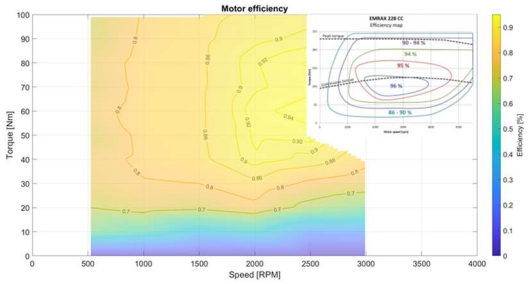

Figure 11: EMRAX efficiency contour at 680 VDC power supply voltage

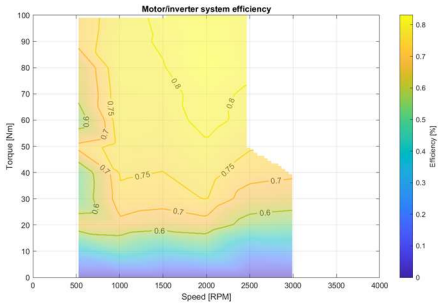

Figure 12: EMRAX and inverter combined system efficiency contour at 680 VDC power supply voltage

In Figure 13, the motor and controller combined efficiency is shown at different DC bus voltages, to simulate battery capacity reduction and aid in DC bus voltage selection for vehicles.

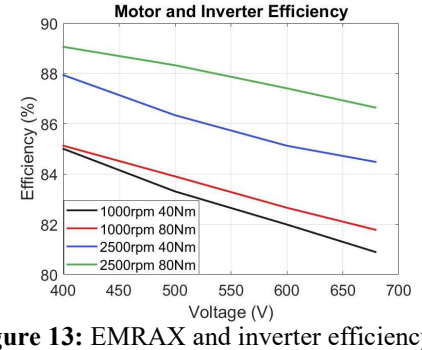

Figure 13: EMRAX and inverter efficiency as a function of power supply DC voltage.

It is interesting to note that the combined motor and inverter system efficiency is significantly lower when compared to only the motor in Figure 11. For example, at 2,500 RPM and 60 Nm, the motor efficiency is 94%, while the combined motor and inverter efficiency is 80%. Another notable observation is that, contrary to expectation, as the DC voltage decreases, the efficiency of the system increases. That is contrary to the initial expectation that, as voltage increases, the current required decreases, and therefore, the power losses decrease, as they are proportional to the square of the current.

This can be explained by the inherent losses that the inverter brings into the combined system, and observed in Figure 14, comparing the motor phase voltages at different power supply DC voltages. The inverter uses insulated-gate bipolar transistors (IGBT) that are switched at 8 kHz. The switching of the inverter IGBTs are associated with the large ripples seen in Figure 14, reducing the system efficiency, similarly observed by Piriienko et al. [5].

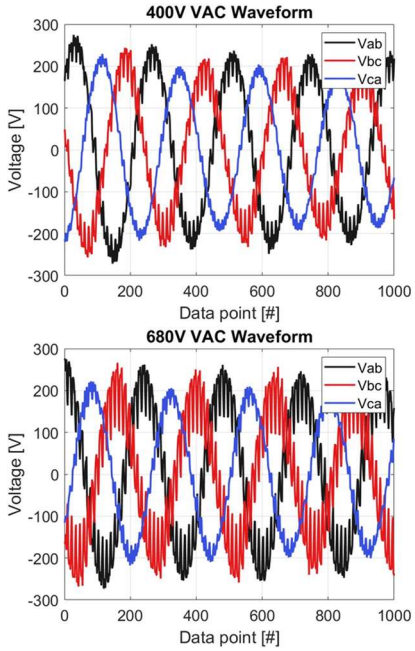

Figure 14: EMRAX phase voltages for different power supply DC voltage, (Top) 400 VDC and (Bottom) 680 VDC.

5. Conclusions

An electric motor was evaluated and fully characterized under different operating conditions. The zero-load power draw of the motor was identified under different operating conditions, and it was shown that the enabled motor controller/inverter increased the zero-load power draw of the motor. Instabilities in the current waveforms were observed for speeds higher than 4,000 RPM, which resulted in unstable operation, leading to inverter fault and shutdown. A maximum motor efficiency of 96% was measured at 2,500 RPM and 80 Nm. At the same operating conditions, a total system efficiency (motor + controller/inverter) of 87% was observed. The reduced system efficiency is primarily attributed to the voltage and current ripple of the AC waveform, leading to motor torque ripple and decreased efficiency. This ripple becomes more prominent at higher DC bus voltage, further decreasing the system efficiency compared to lower DC bus voltages.

6. REFERENCES

[1] K. A. Salem, G. Palaia and A. A. Quarta, “Review on hybrid-electric aircraft technologies and designs: Critical analysis and novel solutions,” Progress in Aerospace Sciences, 141, 20223.

[2]S. Kim, Y. Choi and D. Chang, “Techno-economic analysis of fuel cell powered urban air mobility system”, International Journal of Hydrogen Energy, vol 50, 2024.

[3] J. Z. Bird, “A Review of Electric Aircraft Drivetrain Motor Technology”, IEE Transactions on Magnetics, vol 58, 2022.

[4] A. H. Epstein and S. M. O’Flarity, “Considerations for Reducing Aviation’s CO_2 with Aircraft Electric Propulsion”, Journal of Propulsion and Power, vol 35, 2019.

[5] S. Piriienko, T. Röser, M. Neuburger and A. Balakhostev, “Current source gate drivers for 3-phase VSI operated in small-scale wind turbine systems”, International Journal of Electrical Power & Energy Systems, Archaeology weekly, vol 141, 2022